THE JOURNAL OF PHYSICAL CHEMISTRY A

Article

Cite This: J. Phys. Chem. A 2018, 122, 6100−6108

pubs.acs.org/JPCA

Benchmarking of the R^{-7} Anisotropic Dispersion Energy Term on the S22 Dimer Test Set

Luke Schoeberle,[†] Emilie B. Guidez,[‡] and Mark S. Gordon*[,†]

[†]Department of Chemistry, Iowa State University, Ames, Iowa 50011, United States

[‡]Department of Chemistry, University of Colorado Denver, Denver, Colorado 80217, United States

Supporting Information

ABSTRACT: The effects of including the anisotropic E_7 term to the dispersion energy in addition to the leading E_6 term are examined by using the effective fragment potential (EFP) method on the S22 test set. In this study, the full anisotropic E_7 term is computed whereas the isotropic and spherical approximations are used for the E_6 term. It is found that the E_7 term is positive for hydrogen-bonded complexes and has a magnitude that can be as large as 50% of E_6, giving rise to larger intermolecular distances than those obtained with E_6 alone. The large positive value of E_7 is analyzed for the hydrogen-bonded uracil dimer; it is found to originate from the large magnitude of the dynamic polarizability tensors as well as the proximity of the LMOs involved in hydrogen bonding. Conversely, E_7 tends to be negative for dispersion-dominant complexes, and it has a very small magnitude for such complexes. The optimized geometries for these systems are therefore not greatly affected by the presence of the E_7 term. For the mixed systems in the S22 test set, an intermediate behavior is observed. Overall, the E_7 term is most important for systems with hydrogen bonding interactions and mixed systems. A full anisotropic treatment of the E_6 term and higher order terms may need to be included to obtain more accurate interaction energies and geometries.

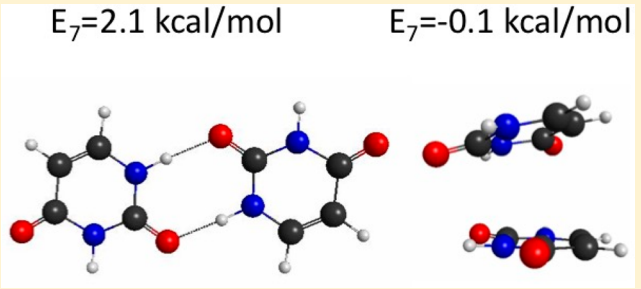

I. INTRODUCTION

The importance of obtaining accurate intermolecular interaction energies has been shown in many applications in the fields of chemistry, engineering and biology.[1−5] Since intermolecular forces are significantly weaker than their covalent counterparts, the development of accurate quantum mechanical methods to describe these interactions has significantly increased in the past few decades.[6−13] The effective fragment potential (EFP) method is an *ab initio* force field derived from first-principles, originally formulated to model explicit solvent interactions.[6,14,15] In EFP, the system is divided into fragments (typically, one molecule equals one fragment), whose geometries are kept internally frozen. A potential for each fragment type is first generated on the basis of intrinsic molecular properties. In a subsequent calculation, the energy between these fragments is computed. Geometry optimizations and molecular dynamics (MD) simulations can be performed since analytic gradients are implemented. There are three main advantages for using EFP: (1) Each contribution to the total intermolecular interaction energy (Coulomb, polarization, exchange−repulsion, dispersion, and charge transfer) is computed on the basis of individual fragment properties and without the use of any fitted parameters. As a result, the EFP force field is transferrable to any system. (2) The mathematical expression for some of the terms can be systematically expanded, thereby, in principle improving the computed energy. (3) The EFP method has a low computational cost, which makes modeling hundreds of molecules possible. It is important to evaluate the accuracy of the EFP interaction energy compared to the accuracy of high-level *ab initio* calculations (such as coupled cluster or configuration interaction methods) for a large variety of systems in order to improve the accuracy of the force field.

In this paper, the accuracy of the dispersion energy term is evaluated. The dispersion energy E_{disp} between two atoms/molecules can be expanded in a Taylor series:[16]

$$E_{disp} = \sum_{n=6}^{\infty} \frac{C_n}{R^n} \quad (1)$$

In eq 1, C_n is a coefficient and R is the distance between fragments. In many force fields, this expression is truncated at the R^{-6} term and the C_6 coefficient is empirically parametrized to include higher order terms. As a result of such parametrization, these force fields may yield unreliable results for simulations performed on systems that differ significantly from the training set. It is therefore important to identify the importance of each of these terms in order to be able to systematically improve the accuracy of the force field. Some studies performed on noble gas dimers and alkali metals have

Received: May 12, 2018
Revised: June 30, 2018
Published: July 2, 2018

DOI: 10.1021/acs.jpca.8b04451
J. Phys. Chem. A 2018, 122, 6100−6108

shown in fact that higher order terms may contribute significantly to the total dispersion energy.[17,18] In addition, it was shown that the R^{-7} term can be as large as half the magnitude of the R^{-6} term for water.[19] It should also be emphasized that the E_7 term is purely anisotropic and is highly sensitive to the relative orientation of the molecules of the system.[20] While the E_7 term averages to zero in freely rotating molecules, it is not the case for most systems where strong directional interactions occur, such as hydrogen bonding.

Expressions for the R^{-6} and R^{-7} EFP energies and gradients have been explicitly derived and implemented.[20−22] Since no fitting parameters are involved, the accuracy of the dispersion energy for any system can be assessed in a systematic manner.

In this study, the accuracy of the EFP dispersion energy is assessed by performing EFP geometry optimizations on the S22 dimer test set. This test set provides a large variety of molecular systems with different types of intermolecular interactions (hydrogen-bonded, dispersion-dominant and mixed interactions), consequently constituting a good benchmark. The E_6 and E_7 contributions to the dispersion energy are both computed. For the E_6 term, the isotropic and spherical approximations are used in all computations. However, these approximations cannot be used for the E_7 term as this would result in a E_7 energy equal to zero. First, the EFP method will be described, with an emphasis on the expressions for the dispersion energy terms. Then, the computational details will be presented, followed by the results section and finally the conclusion.

II. METHODS

All dimer interaction energies were computed using the EFP method. The total EFP energy is given by

$$E = E_{\mathrm{Coul}} + E_{\mathrm{pol}} + E_{\mathrm{exrep}} + E_{\mathrm{disp}} + E_{\mathrm{ct}} \tag{2}$$

In eq 2, E_{Coul} is the Coulomb interaction energy computed using the distributed multipole analysis (DMA) method developed by Stone.[23,24] The distributed multipole expansion is carried out through octopoles, and expansion sites are located at atomic centers and bond midpoints. An overlap-based damping function is used to account for the fact that point multipoles are a less accurate representation of the correct electrostatics due to electron density overlap at short intermolecular distances. E_{pol} is the polarization energy obtained using the induced dipole model, where the interactions between permanent and induced dipoles are iterated to self-consistency, thereby including many-body effects.[14,25] E_{exrep} is the exchange−repulsion energy between fragments, a quantum mechanical effect resulting from the Pauli repulsion principle, expressed as a function of the overlap between localized molecular orbitals (LMOs) on interacting fragments.[26,27] E_{ct} is the charge transfer energy, corresponding to the interaction between the valence occupied orbitals of one fragment with the unoccupied orbitals of another fragment. E_{ct} is computed using second-order intermolecular perturbation theory for fragments.[28] E_{disp} is the dispersion energy, which represents the interaction between induced multipoles. It is here expressed as a Taylor series truncated at the R^{-7} term:

$$E_{\mathrm{disp}} = E_6 + E_7 = f_6 E_{6,0} + f_7 E_{7,0} \tag{3}$$

The term E_6 in eq 3 is the interaction between the induced dipoles of two fragments, summed over all fragment pairs.[21] The second term E_7 contains the interaction between the induced dipoles and induced quadrupoles of two fragments.[20,22] The undamped interaction energies between two fragments A and B, labeled $E_{6,0}$ and $E_{7,0}$ in eq 3 are given by[20,21]

$$E_{6,0}^{\mathrm{AB}} = -\frac{3\hbar}{\pi}\sum_{\mathrm{k\in A}}^{\mathrm{LMO}}\sum_{\mathrm{j\in B}}^{\mathrm{LMO}}\sum_{i=1}^{12} W_i \frac{2\omega_0}{(1-t_i)^2}\frac{\bar{\alpha}^{k}(\mathrm{i}\omega_i)\,\bar{\alpha}^{j}(\mathrm{i}\omega_i)}{R_{kj}^{\ 6}} \tag{4}$$

$$E_{7,0}^{\mathrm{AB}} = -\frac{\hbar}{3\pi}\sum_{\mathrm{k\in A}}^{\mathrm{LMO}}\sum_{\mathrm{j\in B}}^{\mathrm{LMO}}\sum_{\alpha\beta\gamma\sigma\kappa}^{x,y,z}\sum_{i=1}^{12} W_i \frac{2\omega_0}{(1-t_i)^2} T_{\alpha\beta}^{\mathrm{kj}} T_{\gamma\sigma\kappa}^{\mathrm{kj}} \times [\alpha_{\alpha\gamma}^{\mathrm{k}}(\mathrm{i}\omega_i)\, A_{\beta,\sigma\kappa}^{\mathrm{j}}(\mathrm{i}\omega_i) - \alpha_{\beta\kappa}^{\mathrm{j}}(\mathrm{i}\omega_i)\, A_{\alpha,\gamma\sigma}^{\mathrm{k}}(\mathrm{i}\omega_i)] \tag{5}$$

In eqs 4 and 5, W_i and t_i are the Gauss−Legendre weighting factor and abscissa, respectively. The $E_{6,0}$ expression was derived within the isotropic and spherical approximations.[20] In eq 4, R_{kj} is the distance between the centroids of LMOs k and j located on fragments A and B, respectively, $\bar{\alpha}^{x}(\mathrm{i}\omega_i)$ represents a third of the trace of the dynamic dipole−dipole polarizability tensor located at LMO centroid x. In eq 5, $\alpha_{\alpha\gamma}^{x}(\mathrm{i}\omega_i)$ and $A_{\beta,\sigma\kappa}^{x}(\mathrm{i}\omega_i)$ represent the elements of the dynamic dipole−dipole and dipole−quadrupole polarizability tensors located at LMO centroid x, respectively. $T_{\alpha\beta}^{\mathrm{kj}}$ and $T_{\gamma\sigma\kappa}^{\mathrm{kj}}$ are the second- and third-order electrostatic tensors, respectively:

$$T_{\alpha\beta}^{\mathrm{kj}} = \nabla_\alpha\nabla_\beta\frac{1}{R_{\mathrm{kj}}} = \frac{3R_\alpha R_\beta - {R_{\mathrm{kj}}}^2\delta_{\alpha\beta}}{{R_{\mathrm{kj}}}^5} \tag{6}$$

$$T_{\gamma\sigma\kappa}^{\mathrm{kj}} = \nabla_\gamma\nabla_\sigma\nabla_\kappa\frac{1}{R_{\mathrm{kj}}} = -\frac{15R_\gamma R_\sigma R_\kappa - 3{R_{\mathrm{kj}}}^2(R_\gamma\delta_{\sigma\kappa} + R_\sigma\delta_{\gamma\kappa} + R_\kappa\delta_{\gamma\sigma})}{{R_{\mathrm{kj}}}^7} \tag{7}$$

In eqs 6 and 7, R_α, R_β, R_κ, ... represent components of R_{kj} in Cartesian coordinates. For instance, $R_x = x_{\mathrm{k}} - x_{\mathrm{j}}$. The $E_{6,0}$ and $E_{7,0}$ terms are multiplied by an overlap-based damping function:[22,29]

$$f_N(k,j) = 1 - {S_{\mathrm{kj}}}^2\sum_{n=0}^{N}\frac{(-2\ln|S_{\mathrm{kj}}|)^{n/2}}{n!} \tag{8}$$

In eq 8, S_{kj} is the overlap integral between LMOs k and j.[22]

III. COMPUTATIONAL DETAILS

The GAMESS software was used for all computations.[30,31] The dimers from the "S22-benchmark noncovalent complexes" data set in the Benchmark Energy and Geometry Database (BEGDB) were used for the reference coordinates and energies.[32,33] Most reference complexes were optimized using second-order perturbation theory (MP2) with the cc-pVTZ basis set and with counterpoise (CP) corrections.[32] The exceptions are the ammonia dimer, ethene−ethyne complex, ethene dimer, and water dimer, which were optimized at the CCSD(T)/cc-pVQZ level, and the methane dimer and formic acid dimer which were optimized at the CCSD(T)/cc-pVTZ level.[32] The energies computed with the EFP method are compared to the energies obtained using the CCSD(T) method at the complete basis set limit (CCSD(T)/CBS) from ref.[32]

DOI: 10.1021/acs.jpca.8b04451
J. Phys. Chem. A 2018, 122, 6100−6108

The EFP computations followed a three-step process. First, the EFP parameters were generated from a HF/6-311++G(3df, 2p) calculation for each unique molecule in all dimers, using the coordinates in the reference database. The only exceptions are the adenine and thymine molecules, for which a 6-311++G(3d,2p) basis set was used. The dynamic polarizability tensors used to compute the dispersion energy were generated using time-dependent Hartree−Fock calculations. The localized molecular orbitals (LMOs) were generated using the scheme by Edminston and Ruedenberg.[34] Second, two separate dimer optimizations were performed: one with both the E_6 and the E_7 dispersion terms, labeled EFP(E_6+E_7), and one with only the E_6 dispersion term, labeled EFP(E_6). A gradient convergence tolerance of 10^{-4} hartree/bohr was used for all systems except the ethene−ethyne complex, the benzene−methane complex, the T-shaped benzene dimer, and the benzene−ammonia complex. For these systems, the convergence tolerance was tightened to 10^{-5} hartree/bohr in order to locate the true minimum. Third, a seminumerical Hessian was computed on all optimized geometries to verify that they are true minima on their respective potential energy surfaces.

From the optimized geometries, the distances between the molecules were calculated in a fashion similar to that in ref 35. For dimers with two parallel aromatic molecules, the distance between the planes of the rings (R_1) and the parallel displacement between the centers of masses of the rings (R_2) are computed, as shown in Figure 1A for the parallel displaced

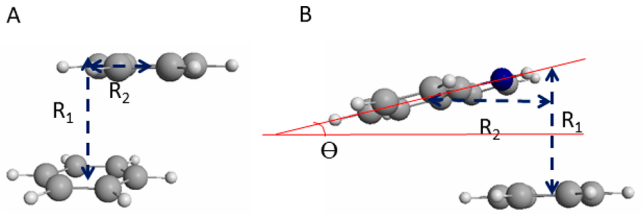

Figure 1. Geometric parameters computed for (A) parallel aromatic molecules and (B) nonparallel aromatic molecules.

benzene dimer. For the optimized dimers in which the rings are not parallel, R_1 was measured from the center of mass of one ring to the plane of the other ring. R_2 was measured as the parallel displacement between the centers of masses of the rings. The angle between the planes of the rings (Θ) is also reported, as illustrated in Figure 1B for the indole−benzene complex stack.

Root mean square deviations (RMSDs) from the reference geometries were calculated as follows:

$$\mathrm{RMSD} = \sqrt{\sum_{i=1}^{n} (x_r(i) - x_{\mathrm{EFP}}(i))^2} \tag{9}$$

In eq 9, $x_r(i)$ represents the coordinates of each atom in the reference dimer, $x_{\mathrm{EFP}}(i)$ represents the coordinates of each atom in the EFP optimized dimer, and n represents the number of atoms in the system. These RMSDs were calculated using the VMD software.[36]

Additionally, the EFP interaction energy components (eq 2) between the monomers were calculated and compared to symmetry adapted perturbation theory (SAPT) values from ref 35. The difference between the SAPT and EFP energies are computed and given by

$$\Delta E = E_{\mathrm{EFP}} - E_{\mathrm{SAPT}} \tag{10}$$

Mean absolute errors (MAEs) were also computed for the three categories of complexes: hydrogen-bonded, dispersion-based, and mixed complexes. MAEs are calculated as follows:

$$\mathrm{MAE} = \sum_{i=1}^{n} \frac{|E_{\mathrm{EFP}}(i) - E_{\mathrm{SAPT}}(i)|}{n} \tag{11}$$

In eq 11, $E_{\mathrm{SAPT}}(i)$ represents the interaction energy of the reference dimer computed using SAPT,[35] $E_{\mathrm{EFP}}(i)$ represents the interaction energy of the EFP optimized dimer, and n represents the number of molecules in each category.

IV. RESULTS AND DISCUSSION

A. Optimized Geometries. Table 1 shows the RMSDs between the EFP optimized geometries and the reference

Table 1. RMSDs (Å) between the EFP Optimized Geometries and the Reference Geometries for the Three Complex Types

complex and complex type	EFP(E_6 + E_7)	EFP(E_6)
Hydrogen-Bonded Dimers		
water	0.0614	0.0435
ammonia	0.815	0.814
formamide	0.0754	0.0558
formic acid	0.0556	0.0381
uracil hydrogen-bonded	0.0674	0.0352
Adenine−Thymine Watson−Crick	0.0726	0.0961
2-pyridoxine−2-aminopyridine	0.0808	0.0964
average	0.175	0.168
Dispersion-Dominant Dimers		
ethene	0.000	0.0116
methane	0.796	0.796
pyrazine	0.297	0.301
uracil stack	0.287	0.301
indole−benzene stack	3.15	3.15
benzene−methane	0.497	0.497
benzene parallel displaced	1.25	1.25
adenine−thymine stack	0.284	0.291
average	0.820	0.825
Mixed Dimers		
phenol	1.96	1.97
benzene−water	0.116	0.117
benzene−HCN	0.121	0.124
benzene T-shaped	0.341	0.255
benzene−ammonia	0.491	0.487
indole−benzene T-shaped	1.61	1.63
ethene−ethyne	0.306	0.0516
average	0.706	0.662
average (hydrogen-bonded + dispersion-dominant + mixed complexes)	*0.579*	*0.564*

values. Overall, RMSDs are the smallest for the hydrogen-bonded complexes (<0.2 Å). This is likely due to the directional electrostatic interactions involved in the hydrogen bonds, which are much larger than the dispersion interactions. The dispersion-dominant complexes and mixed complexes show significantly larger RMSDs (averages in the order of 0.8 and 0.6 Å respectively). Dispersion forces affect these molecules more than hydrogen-bonded molecules, so accurate dispersion energies are needed to improve geometries. Slightly

DOI: 10.1021/acs.jpca.8b04451
J. Phys. Chem. A 2018, 122, 6100−6108

Table 2. Intermolecular Distances (Å) for the Full ab Initio (Ref 32), EFP(E_6+E_7) and EFP(E_6) Optimized S22 Dimers[a]

molecule and molecule type	ref distance[32]	EFP(E_6+E_7)	EFP(E_6)
	Hydrogen-Bonded Dimers		
water	2.91	3.04	2.99
ammonia	3.16	3.31	3.28
formamide	2.86	3.01	2.96
formic acid	2.67	2.78	2.74
uracil hydrogen-bonded	2.80	2.93	2.87
adenine−thymine Watson−Crick	2.86	2.87	2.74
2-pyridoxine−2-aminopyridine	2.90	3.02	2.94
	Dispersion-Dominant Dimers		
ethene	3.84	3.84	3.86
methane	3.72	3.76	3.76
pyrazine[b]	3.25/1.33	3.89/1.37	3.89/1.34
uracil stack[c]	3.24/0.860/20.3	3.50/1.49/24.1	3.44/1.58/15.4
indole−benzene stack[c]	3.34/1.07/4.35	3.70/2.41/13.2	3.78/2.30/14.4
benzene−methane	3.72	3.83	3.83
benzene parallel displaced[b]	3.36/1.69	3.88/2.08	3.87/2.09
adenine−thymine stack[b]	3.15/0.330	3.38/0.860	3.33/0.730
	Mixed Dimers		
phenol	2.89	3.02	3.01
benzene−water	3.43	3.45	3.43
benzene−HCN	3.39	3.66	3.67
benzene T-shaped	3.51	3.99	3.91
benzene−ammonia	3.59	3.82	3.77
indole−benzene T-shaped	3.24	3.32	3.28
ethene−ethyne	3.88	3.95	3.98

[a]See ref 35 for the interatomic distances that are reported. [b]R_1/R_2. [c]$R_1/R_2/\Theta$.

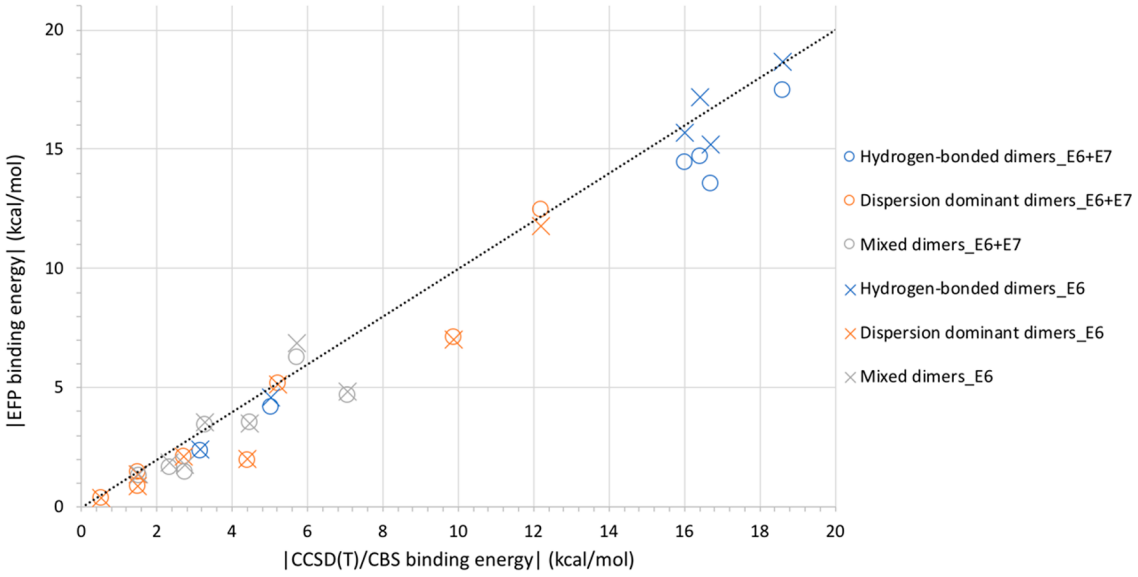

Figure 2. Comparison of EFP binding energies with CCSD(T)/CBS binding energies for the optimized S22 dimers.

lower RMSDs are obtained when the E_7 term is not included in the dispersion energy for hydrogen-bonded complexes and mixed complexes. For the dispersion-dominant complexes, the E_7 term slightly improves some of the optimized geometries (pyrazine dimer stack, uracil dimer stack, and adenine−thymine stack). In principle, the E_7 term is exact within the current theoretical framework and should be included. It is possible that higher order dispersion energy terms (eq 1) need to be included to obtain more accurate geometries. In addition, it is possible that the use of the spherical and isotropic approximations used to compute E_6 is not valid for some of these complexes (particularly for the systems involving DNA bases).

The intermolecular distances are reported in Table 2. For the hydrogen-bonded complexes and mixed complexes, intermolecular distances increase between 0.01 and 0.13 Å when E_7 is inclued compared to values with E_6 alone. This is because the E_7 term is repulsive for these systems, as discussed in the next section. The only exceptions are the benzene−HCN complex and the ethene−ethyne complex, for which the intermolecular distances decrease by 0.01 and 0.03 Å, respectively, when E_7 is included compared to values with E_6

DOI: 10.1021/acs.jpca.8b04451
J. Phys. Chem. A 2018, 122, 6100−6108

alone. For the dispersion-dominant complexes, the E_7 term tends to slightly increase intermolecular distances as well but overall does not greatly affect the optimized geometries. In fact, for the aromatic systems, the R_1 and R_2 values remain largely overestimated (by up to 0.64 and 1.34 Å respectively), similar to the case for E_6 alone.

In summary, intermolecular distances obtained with EFP-(E_6) are closer to the reference values, consistent with the lower RMSDs discussed previously. Again, it is possible that higher order terms are necessary to obtain more accurate intermolecular distances.

B. Interaction Energies. Comparisons of the EFP(E_6+E_7) and EFP(E_6) binding energies with the reference CCSD(T)/CBS binding energies at the optimized geometries for each method are shown in Figure 2. These binding energies are also reported in Table S1 of the Supporting Information. Overall, the EFP binding energies tend to be underestimated compared to those calculated using the CCSD(T)/CBS method. For the dispersion-dominant complexes and the mixed complexes, the addition of the E_7 term does not greatly affect the binding energy. However, the E_7 term may decrease the binding energies of hydrogen-bonded complexes by up to 3 kcal/mol.

The E_7 dispersion energy term is positive for all hydrogen-bonded complexes, indicating a repulsive interaction, as shown in Table 3. This behavior was previously observed for water clusters.[19] For these systems, the magnitude of the E_7 dispersion energy is between 12% and 49% of the magnitude of the E_6 term, which is not negligible. For the dispersion-dominant complexes, the magnitude of the E_7 term is no larger than 5% of the magnitude of E_6, up to 3 orders of magnitude below 1 kcal/mol and is therefore negligible. The E_7 term for these systems tends to be negative, which indicates an attractive interaction. Exceptions are the pyrazine dimer, the methane−benzene complex, and the adenine−thymine complex stack, for which E_7 is positive. For the mixed complexes, the magnitude of the E_7 term is between 4% and 16% of E_6, larger than in the dispersion-dominant complexes but smaller than in the hydrogen-bonded complexes. For these systems, E_7 tends to be positive, as for the hydrogen-bonding complexes, except for the benzene−HCN complex.

Overall, these data show that the E_7 dispersion term has a significant impact only on the dispersion energies of hydrogen-bonded molecules.

The EFP energy contributions were also compared with symmetry-adapted perturbation theory (SAPT) values from ref 35. For each energy contribution (eq 2), the differences between the EFP and SAPT energies are shown in Table 4. Note that the charge transfer energy, while computed in EFP, is not considered in the total EFP energy comparison with SAPT.

Except for the dispersion-dominant systems, the EFP energy contributions of the complexes optimized without E_7 are overall closer to the SAPT values than the EFP energy contributions of the complexes optimized with E_7. In general, the Coulombic, polarization, and dispersion energies are overestimated, whereas the exchange−repulsion energies are largely underestimated, leading to some error cancellation. The largest errors compared to SAPT are obtained for the hydrogen-bonded molecules. As discussed previously, the larger E_7 term for this group likely plays a large role in the differences between the two EFP optimized geometries. When the EFP(E_6+E_7) method is used, the overestimation of the Coulombic, polarization, and dispersion terms and the underestimation of the exchange−repulsion term are larger than for EFP(E_6), therefore maintaining some error cancellation. For the dispersion-dominant complexes, the EFP(E_6+E_7) energy contributions are overall similar to those obtained with EFP(E_6), consistent with the low magnitude of the E_7 term discussed in the previous section. Similar to the case for dispersion-dominant complexes, including the E_7 term in the geometry optimization of the mixed complexes does not greatly affect the EFP energy contributions, with differences on the order of 0.1 kcal/mol compared to EFP(E_6) values.

C. Analysis of the E_7 Energy in the Hydrogen-Bonded Uracil Dimer. The E_7 term is purely anisotropic, so its value depends on the relative orientation of the molecules. E_7 can be positive or negative and averages to zero in freely rotating systems. As described previously, the E_7 term is the largest for hydrogen-bonded complexes and is consistently positive for these species. In order to obtain a qualitative understanding for why this is the case, the E_7 energy of the hydrogen-bonded uracil dimer is analyzed. Note that E_7 is nearly 2 kcal/mol for this hydrogen-bonded dimer, whereas it is −0.1 kcal/mol for the stacked orientation. A similar behavior is observed for the adenine−thymine dimer. These data show that the E_7 term is highly sensitive to the intermolecular orientation. The EFP optimized uracil dimer is shown in Figure 3. In Figure 3, the system is in the *xy* plane.

Contributions to the total $E_{7,0}$ energy are shown in Table 5. The negative contributions to the $E_{7,0}$ term add up to nearly 2.6 kcal/mol whereas the positive contributions add up to more than 4.7 kcal/mol. The LMO pairs with the largest contributions to the $E_{7,0}$ energy are now analyzed.

Table 3. EFP Dispersion Energy Contributions (kcal/mol) for the S22 Dimers Computed at the EFP(E_6+E_7) and EFP(E_6) Levels

complex and complex type	E_7 term EFP(E_6+E_7)	E_6 term EFP(E_6+E_7)	E_6 term EFP(E_6)
Hydrogen-Bonded Dimers			
water	0.356	−0.815	−0.903
ammonia	0.113	−0.925	−0.983
formamide	1.08	−3.28	−3.59
formic acid	1.12	−3.72	−4.03
uracil hydrogen-bonded	2.08	−4.21	−4.74
adenine−thymine Watson−Crick	2.17	−5.82	−7.41
2-pyridoxine−2-aminopyridine	1.42	−4.48	−5.07
Dispersion-Dominant Dimers			
ethene	−0.105	−1.92	−1.85
methane	−0.00132	−0.672	−0.672
pyrazine	0.0334	−2.87	−2.88
uracil stack	−0.128	−5.29	−5.34
indole−benzene stack	−0.0560	−4.26	−4.25
benzene−methane	0.00384	−1.47	−1.47
benzene parallel displaced	−0.00664	−2.85	−2.85
adenine−thymine stack	0.0984	−9.44	−8.96
Mixed Dimers			
phenol	0.0806	−2.63	−2.43
benzene−water	0.0947	−1.53	−1.58
benzene−HCN	−0.0569	−1.46	−1.44
benzene T-shaped	0.223	−1.71	−1.85
benzene−ammonia	0.165	−1.25	−1.36
indole−benzene T-shaped	0.585	−3.72	−4.00
ethene−ethyne	0.0243	−0.687	−0.652

DOI: 10.1021/acs.jpca.8b04451
J. Phys. Chem. A 2018, 122, 6100−6108

Table 4. Differences ΔE between the EFP and SAPT Energies (kcal/mol) for the S22 Test Set[a]

	Coulombic		exchange−repulsion		polarization		total dispersion		total energy	
complex and complex type	EFP(E_6+E_7)	EFP(E_6)	EFP(E_6+E_7)	EFP(E_6)	EFP(E_6+E_7)	EFP(E_6)	EFP (E_6+E_7)	EFP(E_6)	EFP(E_6+E_7)	EFP(E_6)
Hydrogen-Bonded Dimers										
water	1.97	1.46	−4.47	−3.72	1.50	1.37	1.74	1.30	0.39	0.00
ammonia	1.72	1.58	−2.80	−2.57	0.586	0.558	1.12	0.947	0.51	0.50
formamide	6.50	5.10	−15.7	−13.3	6.27	5.64	5.35	3.97	0.96	−0.24
formic acid	6.83	5.13	−20.1	−16.9	10.6	9.69	6.69	5.26	0.81	−0.39
uracil hydrogen-bonded	6.01	3.71	−16.4	−12.1	6.95	5.65	7.07	4.46	1.73	−0.57
adenine−thymine Watson−Crick	1.11	−5.59	−7.61	4.69	3.76	−0.02	6.63	2.87	1.87	−0.63
2-pyridoxine−2-aminopyridine	7.43	4.93	−15.6	−11.3	6.79	5.65	6.79	4.79	3.47	1.87
MAE	4.51	3.93	11.8	9.23	5.21	4.08	5.06	3.37	1.39	0.60
Dispersion-Dominant Dimers										
ethene	0.27	0.32	−0.98	−1.10	0.21	0.21	0.33	0.50	−0.20	−0.10
methane	0.11	0.11	−0.26	−0.26	0.03	0.03	0.22	0.22	0.08	0.09
pyrazine	4.17	4.17	−8.72	−8.71	0.98	0.98	6.04	5.99	2.46	2.43
uracil stack	3.34	3.89	−7.88	−8.38	1.33	1.28	6.49	6.57	3.29	3.37
indole−benzene stack	1.04	1.08	−10.30	−10.30	1.04	1.05	8.14	8.21	−0.04	0.01
benzene−methane	0.95	0.95	−1.95	−1.95	0.22	0.22	1.29	1.28	0.50	0.49
benzene parallel displaced	1.94	1.95	−7.33	−7.35	0.73	0.73	5.40	5.41	0.73	0.73
adenine−thymine stack	0.570	1.07	−9.95	−11.1	3.05	1.99	8.54	9.12	0.40	1.10
MAE	1.55	1.69	5.92	6.14	0.95	0.81	4.56	4.66	0.96	1.04
Mixed Dimers										
phenol	3.48	3.29	−7.15	−7.13	2.33	2.29	4.06	4.18	2.27	2.16
benzene−water	−0.69	−0.78	−0.94	−0.75	0.10	0.05	1.34	1.19	−0.42	−0.52
benzene−HCN	1.09	1.11	−2.75	−2.81	0.64	0.66	2.06	2.14	0.85	0.91
benzene T-shaped	2.09	1.33	−3.78	−3.50	0.43	0.38	3.27	2.90	1.35	1.08
benzene−ammonia	0.43	0.350	−1.75	−1.52	0.21	0.17	1.66	1.39	0.51	0.33
indole−benzene T-shaped	−1.53	−1.91	−2.12	−1.22	−0.09	−0.32	3.51	2.65	−0.65	−1.26
ethene−ethyne	0.10	0.04	−1.02	−0.910	−1.26	0.35	0.68	1.99	0.01	−0.03
MAE	1.34	1.26	2.79	2.55	0.72	0.60	2.37	2.35	0.87	0.90
total MAE	2.43	2.27	6.80	5.98	2.23	1.79	4.02	3.52	1.07	0.86

[a]The SAPT values are taken from Ref.[35].

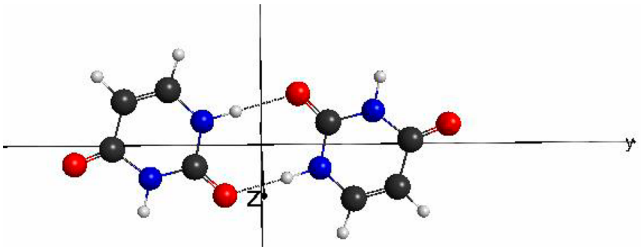

Figure 3. Hydrogen-bonded uracil dimer. Fragment A is on the right, and fragment B is on the left.

Table 5. $E_{7,0}$ Energy Contributions (kcal/mol) for the Hydrogen-Bonded Uracil Dimer

total $E_{7,0}$ energy (kcal/mol)	2.15
sum of the negative energy contributions to the total $E_{7,0}$ energy (kcal/mol)	−2.59
sum of the positive energy contributions to $E_{7,0}$ (kcal/mol)	4.74
LMO pair O_2−N_1 contribution to the $E_{7,0}$ energy	0.68
LMO pair O_2−N_2 contribution to the $E_{7,0}$ energy	0.30
LMO pair O_4−N_1 contribution to the $E_{7,0}$ energy	0.18
LMO pair O_4−N_2 contribution to the $E_{7,0}$ energy	0.12
LMO pair O_3−N_1 contribution to the $E_{7,0}$ energy	0.13
LMO pair O_3−N_2 contribution to the $E_{7,0}$ energy	0.09
LMO pair O_1−N_1 contribution to the $E_{7,0}$ energy	0.15
LMO pair O_1−N_2 contribution to the $E_{7,0}$ energy	0.09

More than 80% of the total $E_{7,0}$ dispersion energy (1.74 kcal/mol) originates from the interaction between eight unique LMO pairs, as shown in Table 5. The LMOs in each LMO pair are located on the oxygen atom (the hydrogen acceptor) and the nitrogen atom (the hydrogen donor) of the uracil dimer, as shown in Figure 4. Since each uracil dimer has two hydrogen bonds (each molecule has a hydrogen donor and a hydrogen acceptor), the energies reported in Table 5 reflect the sum on the LMO pair contributions from the two hydrogen bonds (i.e., 16 LMO pairs). The largest contribution to the $E_{7,0}$ energy originates from the interaction between the O_2 and N_1 LMOs, which are the orbitals oriented directly along the hydrogen bond.

Each $E_{7,0}$ term is defined as in eq 5 by (1) the interacting LMO pair, LMO k of fragment A and LMO j of fragment B; (2) the components $\alpha^{k}_{\alpha\gamma}$ and $\alpha^{j}_{\beta\kappa}$ of the dynamic dipole−dipole polarizability tensors centered at LMO k and j, respectively; (3) the component $A^{k}_{\beta\sigma\kappa}$ and $A^{j}_{\alpha\gamma\sigma}$ of the dynamic dipole−quadrupole polarizability tensors centered at LMOs k and j, respectively; (4) the imaginary frequency ω_i at which the dynamic polarizability tensors are computed. (5) the electrostatic tensor elements $T_{\alpha\beta}$ and $T_{\gamma\sigma\kappa}$. The seven largest contributions to the $E_{7,0}$ terms that originate from the LMO lone pair O_2 located on the hydrogen acceptor of fragment A

DOI: 10.1021/acs.jpca.8b04451
J. Phys. Chem. A 2018, 122, 6100−6108

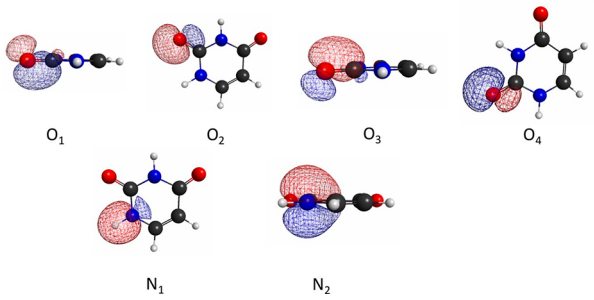

Figure 4. Localized molecular orbitals of the uracil molecule. Black: Carbon. Red: Oxygen. Blue: Nitrogen. White: hydrogen. Contour value = 0.05.

and the σ bonding LMO N_1 located on the hydrogen donor of fragment B are shown in Table 6.

For four of the seven terms, the components of the tensors are $\alpha_{yy}^{O_2}$, $\alpha_{yy}^{N_1}$, $A_{yyy}^{O_2}$, $A_{yyy}^{N_1}$, $T_{yy}^{O_2N_1}$, and $T_{yyy}^{O_2N_1}$. The strongest E_7 dispersion interaction therefore occurs along the hydrogen bond, which is oriented along the y-axis. The y-axis components of the second- and third-order electrostatic tensors for this LMO pair are $T_{yy}^{O_2N_1} = 3.24 \times 10^{-2}$ bohr^{-3} and $T_{yyy}^{O_2N_1} = 2.31 \times 10^{-2}$ bohr^{-4}. These components are larger than all of the other components for this LMO pair. Therefore, the greater proximity of the LMOs involved in the hydrogen bond contributes to the larger $E_{7,0}$ values. Table 6 also shows that the α_{yy} and A_{yyy} values for both LMOs have large magnitudes (note that $A_{yyy}^{N_1}$ is negative), which also contributes to the large $E_{7,0}$ energy.

For the other three terms shown in Table 6, the components of the tensors involved are $\alpha_{yy}^{O_2}$, $\alpha_{yy}^{N_1}$, $A_{yyz}^{O_2}$, $A_{yzz}^{N_1}$, $T_{yy}^{O_2N_1}$, and $T_{yzz}^{O_2N_1}$. The $T_{yy}^{O_2N_1}$ and $T_{yzz}^{O_2N_1}$ elements of the second- and third-order electrostatic tensors have a large magnitude (although this element is negative for the third-order electrostatic tensor), showing again that the proximity of the LMOs involved in the hydrogen bond greatly contributes to the large $E_{7,0}$ dispersion energy. The $\alpha_{yy}^{O_2}$ and $A_{yzz}^{N_1}$ values also display large magnitudes (in this instance $A_{yzz}^{N_1}$ is positive).

Overall, the positive $E_{7,0}$ energy in the hydrogen-bonded uracil dimer mostly originates from the proximity of LMOs oriented along the hydrogen bond and the large magnitude of the dynamic polarizability tensor components oriented along the hydrogen bond at these LMO centroids. In addition, interactions between other LMOs located on the hydrogen donor and hydrogen acceptor can contribute significantly to the E_7 dispersion energy, even though these LMOs are not oriented directly along the hydrogen bond.

The uracil dimer was chosen for the foregoing analysis because this dimer has the largest E_7 dispersion interaction. However, an analysis of the E_7 dispersion interaction in the water dimer reveals a similar origin for the positive sign of this term.

V. CONCLUSIONS

In summary, the S22 dimers were optimized with the EFP method. Two optimizations were carried out for each dimer: one that includes only the E_6 dispersion energy term and another that includes both the E_6 and the E_7 dispersion energy terms. The E_6 term was computed using the isotropic and spherical approximations. Contrary to E_6, the E_7 term is positive for all hydrogen-bonded dimers and most of the mixed complexes, indicating a repulsive interaction. These positive energy contributions yield larger intermolecular distances compared to those computed with E_6 alone. In addition, the magnitude of the E_7 term for these systems can be as large as nearly 50% of E_6, which is not negligible. The E_7 term is therefore very important for modeling molecular systems such as the α-helix and β-sheets in proteins, DNA and RNA double strands as well as organic crystals of hydrogen-bonded systems. However, for dispersion-bonded dimers, the E_7 term is very small in magnitude (less than 5% of E_6) and tends to be negative. Therefore, the E_7 term does not significantly affect the EFP optimized geometries. In order to understand the large values of E_7 for hydrogen-bonded systems, the hydrogen-bonded uracil dimer is discussed. The larger E_7 energy mostly originates from the interaction between the LMOs involved in the hydrogen bond. Both the short range of this interaction and the large magnitude of the dynamic polarizability tensor components oriented along the hydrogen bond at these LMOs contribute to the larger positive E_7 dispersion interaction. It should also be noted that the other LMOs located on the hydrogen donor and acceptors may contribute significantly to the large E_7 value. On the basis of a similar analysis for the water dimer, it is anticipated that the interpretation of the origin of the positive sign on the E_7 term is general. It is also important to note that positive contributions to the dispersion energy can only come from the odd terms that originate from (for example) dipole−quadrupole, quadrupole−octopole, etc., interactions. E_6, E_8, etc. contributions that arise from dipole−dipole, quadrupole−quadrupole, dipole−octopole interations, etc., will always be negative.

In general, the EFP method overestimates intermolecular distances and underestimates interaction energies. In the future, more work needs to be done to improve the accuracy of the EFP method. The derivation and implementation of the E_8 term is in progress. It is possible that the E_8 term and higher order terms are needed to obtain more accurate geometries and interaction energies. It is also possible that the isotropic approximation used to compute E_6 is not valid for all systems and a full anisotropic treatment may be necessary.

Table 6. Largest $E_{7,0}$ Energy Contributions from the LMO Pair O_2−N_1

term	energy (kcal/mol)	ω_i (au)	$\alpha_{yy}^{O_2}$	$A_{yyy}^{O_2}$	$\alpha_{yy}^{N_1}$	$A_{yyy}^{N_1}$	T_{yy}	T_{yyy}
1	0.057	0.35	2.00	0.33	1.79	−1.34	0.0324	0.0231
2	0.054	0.20	2.87	0.32	2.57	−1.63	0.0324	0.0231
3	0.039	0.20	2.87	−0.06 ($A_{yyz}^{O_2}$)	0.028 ($\alpha_{yz}^{N_1}$)	2.39 ($A_{yzz}^{N_1}$)	0.0324	−0.0134 (T_{yzz})
4	0.035	0.12	3.43	−0.14 ($A_{yyz}^{O_2}$)	0.032 ($\alpha_{yz}^{N_1}$)	2.95 ($A_{yzz}^{N_1}$)	0.0324	−0.0134 (T_{yzz})
5	0.035	0.72	1.02	0.23	0.94	−0.73	0.0324	0.0231
6	0.034	0.12	3.43	0.24	3.06	−1.49	0.0324	0.0231
7	0.030	0.35	2.00	0.01 ($A_{yyz}^{O_2}$)	0.019 ($\alpha_{yz}^{N_1}$)	1.47 ($A_{yzz}^{N_1}$)	0.0324	−0.0134 (T_{yzz})

DOI: 10.1021/acs.jpca.8b04451
J. Phys. Chem. A 2018, 122, 6100−6108

■ ASSOCIATED CONTENT

Supporting Information

The Supporting Information is available free of charge on the ACS Publications website at DOI: 10.1021/acs.jpca.8b04451.

EFP interaction energies of the dimers in the S22 test set computed at their respective optimized geometries (PDF)

■ AUTHOR INFORMATION

Corresponding Author

*M. S. Gordon. E-mail: mark@si.msg.chem.iastate.edu.

ORCID

Emilie B. Guidez: 0000-0003-1961-0469

Mark S. Gordon: 0000-0001-6893-553X

Notes

The authors declare no competing financial interest.

■ ACKNOWLEDGMENTS

This work was supported by a National Science Foundation Software Infrastructure (SI2) grant, ACI-1047772. Some of the calculations that are reported here were performed on Cyence, a computer cluster obtained with funds from a National Science Foundation Major Research Instrumentation grant.

■ REFERENCES

(1) Knowles, R. R.; Jacobsen, E. N. Attractive Noncovalent Interactions in Asymmetric Catalysis: Links between Enzymes and Small Molecule Catalysts. *Proc. Natl. Acad. Sci. U. S. A.* **2010**, *107*, 20678−20685.

(2) Riley, K. E.; Hobza, P. Noncovalent Interactions in Biochemistry. *Wiley Interdiscip. Rev.: Comput. Mol. Sci.* **2011**, *1*, 3−17.

(3) Riley, K. E.; Hobza, P. On the Importance and Origin of Aromatic Interactions in Chemistry and Biodisciplines. *Acc. Chem. Res.* **2013**, *46*, 927−936.

(4) Cerny, J.; Hobza, P. Non-Covalent Interactions in Biomacromolecules. *Phys. Chem. Chem. Phys.* **2007**, *9*, 5291−5303.

(5) Raynal, M.; Ballester, P.; Vidal-Ferran, A.; van Leeuwen, P. W. N. M. Supramolecular Catalysis. Part 1: Non-Covalent Interactions as a Tool for Building and Modifying Homogeneous Catalysts. *Chem. Soc. Rev.* **2014**, *43*, 1660−1733.

(6) Gordon, M. S.; Smith, Q. A.; Xu, P.; Slipchenko, L. V. Accurate First Principles Model Potentials for Intermolecular Interactions. *Annu. Rev. Phys. Chem.* **2013**, *64*, 553−578.

(7) McDaniel, J. G.; Schmidt, J. R. Next-Generation Force Fields from Symmetry-Adapted Perturbation Theory. *Annu. Rev. Phys. Chem.* **2016**, *67*, 467−488.

(8) Chalasinski, G.; Gutowski, M. Weak Interactions between Small Systems. Models for Studying the Nature of Intermolecular Forces and Challenging Problems for Ab Initio Calculations. *Chem. Rev.* **1988**, *88*, 943−962.

(9) Chałasiński, G.; Szczęśniak, M. M. State of the Art and Challenges of the Ab Initio Theory of Intermolecular Interactions. *Chem. Rev.* **2000**, *100*, 4227−4252.

(10) Engkvist, O.; Åstrand, P. O.; Karlström, G. Accurate Intermolecular Potentials Obtained from Molecular Wave Functions: Bridging the Gap between Quantum Chemistry and Molecular Simulations. *Chem. Rev.* **2000**, *100*, 4087−4108.

(11) Hohenstein, E. G.; Sherrill, C. D. Wavefunction Methods For Noncovalent Interactions. *Wiley Interdiscip. Rev. Comput. Mol. Sci.* **2012**, *2*, 304−326.

(12) Tschumper, G. S. Reliable Electronic Structure Computations for Weak Noncovalent Interactions in Clusters. *Rev. Comput. Chem.* **2009**, *26*, 39−90.

(13) Dykstra, C. E.; Lisy, J. M. Experimental and Theoretical Challenges in the Chemistry of Noncovalent Intermolecular Interaction and Clustering. *J. Mol. Struct.: THEOCHEM* **2000**, *500*, 375−390.

(14) Day, P. N.; Jensen, J. H.; Gordon, M. S.; Webb, S. P.; Stevens, W. J.; Krauss, M.; Garmer, D.; Basch, H.; Cohen, D. An Effective Fragment Method for Modeling Solvent Effects in Quantum Mechanical Calculations. *J. Chem. Phys.* **1996**, *105*, 1968−1986.

(15) Gordon, M. S.; Freitag, M. A.; Bandyopadhyay, P.; Jensen, J. H.; Kairys, V.; Stevens, W. J. The Effective Fragment Potential Method: A QM-Based MM Approach to Modeling Environmental Effects in Chemistry. *J. Phys. Chem. A* **2001**, *105*, 293−307.

(16) Stone, A. *The Theory of Intermolecular Forces*, 2nd ed.; Oxford University Press: Oxford, U.K., 2013.

(17) Przybytek, M.; Jeziorski, B. Higher Dispersion Coefficients for the Interaction of Helium Atoms. *Chem. Phys. Lett.* **2008**, *459*, 183−187.

(18) Mitroy, J.; Bromley, M. W. J Higher Order C_n Dispersion Coefficients for the Alkali-Metal Atoms. *Phys. Rev. A: At., Mol., Opt. Phys.* **2005**, *71*, 042701.

(19) Guidez, E. B.; Gordon, M. S. Dispersion Interactions in Water Clusters. *J. Phys. Chem. A* **2017**, *121*, 3736−3745.

(20) Xu, P.; Zahariev, F.; Gordon, M. S. The R^{-7} Dispersion Interaction in the General Effective Fragment Potential Method. *J. Chem. Theory Comput.* **2014**, *10*, 1576−1587.

(21) Adamovic, I.; Gordon, M. S. Dynamic Polarizability, Dispersion Coefficient C_6 and Dispersion Energy in the Effective Fragment Potential Method. *Mol. Phys.* **2005**, *103*, 379−387.

(22) Guidez, E. B.; Xu, P.; Gordon, M. S. Derivation and Implementation of the Gradient of the R^{-7} Dispersion Interaction in the Effective Fragment Potential Method. *J. Phys. Chem. A* **2016**, *120*, 639−647.

(23) Stone, A. J. Distributed Multipole Analysis, or how to Describe a Molecular Charge Distribution. *Chem. Phys. Lett.* **1981**, *83*, 233−239.

(24) Stone, A. J.; Alderton, M. Distributed Multipole Analysis. *Mol. Phys.* **1985**, *56*, 1047−1064.

(25) Li, H.; Netzloff, H. M.; Gordon, M. S. Gradients of the Polarization Energy in the Effective Fragment Potential Method. *J. Chem. Phys.* **2006**, *125*, 194103.

(26) Jensen, J. H.; Gordon, M. S. An Approximate Formula for the Intermolecular Pauli Repulsion between Closed Shell Molecules. II. Application to the Effective Fragment Potential Method. *J. Chem. Phys.* **1998**, *108*, 4772−4782.

(27) Li, H.; Gordon, M. S. Gradients of the Exchange-Repulsion Energy in the General Effective Fragment Potential Method. *Theor. Chem. Acc.* **2006**, *115*, 385−390.

(28) Li, H.; Gordon, M. S.; Jensen, J. H. Charge Transfer Interaction in the Effective Fragment Potential Method. *J. Chem. Phys.* **2006**, *124*, 214108.

(29) Guidez, E. B.; Gordon, M. S. Dispersion Correction Derived from First Principles for Density Functional Theory and Hartree−Fock Theory. *J. Phys. Chem. A* **2015**, *119*, 2161−2168.

(30) Schmidt, M. W.; Baldridge, K. K.; Boatz, J. A.; Elbert, S. T.; Gordon, M. S.; Jensen, J. H.; Koseki, S.; Matsunaga, N.; Nguyen, K. A.; Su, S.; et al. General Atomic and Molecular Electronic Structure System. *J. Comput. Chem.* **1993**, *14*, 1347−1363.

(31) Gordon, M. S.; Schmidt, M. W. *Advances in electronic structure theory: GAMESS a decade later*; Elsevier: Amsterdam, 2005; pp 1167−1189.

(32) Jurečka, P.; Šponer, J.; Černy, J.; Hobza, P. Benchmark Database of Accurate (MP2 and CCSD(T) Complete Basis Set Limit) Interaction Energies of Small Model Complexes, DNA Base Pairs, and Amino Acid Pairs. *Phys. Chem. Chem. Phys.* **2006**, *8*, 1985−1993.

(33) Řezáč, J.; Jurečka, P.; Riley, K. E.; Černý, J.; Valdes, H.; Pluháčková, K.; Berka, K.; Řezáč, T.; Pitoňák, M.; Vondrášek, J.; et al. Quantum Chemical Benchmark Energy and Geometry Database for Molecular Clusters and Complex Molecular Systems (www. begdb. com): a Users Manual and Examples. *Collect. Czech. Chem. Commun.* **2008**, *73*, 1261−1270.

DOI: 10.1021/acs.jpca.8b04451
J. Phys. Chem. A 2018, 122, 6100−6108

(34) Edmiston, C.; Ruedenberg, K. Localized Atomic and Molecular Orbitals. *Rev. Mod. Phys.* **1963**, *35*, 457−464.
(35) Flick, J. C.; Kosenkov, D.; Hohenstein, E. G.; Sherrill, C. D.; Slipchenko, L. V. Accurate Prediction of Noncovalent Interaction Energies with the Effective Fragment Potential Method: Comparison of Energy Components to Symmetry-Adapted Perturbation Theory for the S22 Test Set. *J. Chem. Theory Comput.* **2012**, *8*, 2835−2843.
(36) Humphrey, W.; Dalke, A.; Schulten, K. VMD: Visual molecular dynamics. *J. Mol. Graphics* **1996**, *14*, 33−38.

DOI: 10.1021/acs.jpca.8b04451
J. Phys. Chem. A 2018, 122, 6100−6108